Journal of South American Earth Sciences 64 (2015) 152–165

Contents lists available at ScienceDirect

Journal of South American Earth Sciences

journal homepage: www.elsevier.com/locate/jsames

Successive reactivation of older structures under variable heat flow conditions evidenced by K–Ar fault gouge dating in Sierra de Ambato, northern Argentine broken foreland

Julieta C. Nóbile [a, *], Gilda Collo [a], Federico M. Dávila [a], Federico Martina [a], Klaus Wemmer [b]

[a] Centro de Investigaciones en Ciencias de La Tierra, CONICET-UNC, Av. Vélez Sarsfield 1611, Córdoba, Argentina
[b] Geoscience Centre, Georg-August University, Goldschmidtstraße 3, 37077 Göttingen, Germany

ARTICLE INFO

Article history:
Received 27 November 2014
Received in revised form
8 October 2015
Accepted 12 October 2015
Available online 23 October 2015

Keywords:
Argentine broken foreland
K–Ar dating
Fault gouge dating
Clay mineral geochronology

ABSTRACT

The Argentine broken foreland has been the subject of continuous research to determine the uplift and exhumation history of the region. High-elevation mountains are the result of N–S reverse faults that disrupted a W–E Miocene Andean foreland basin. In the Sierra de Ambato (northern Argentine broken foreland) the reverse faults offset Neogene sedimentary rocks (Aconquija Fm., ~9 Ma) and affect the basement comprising Paleozoic metamorphic rocks that have been dated at ~477–470 Ma. In order to establish a chronology of these faults affecting the previous continuous basin we date the formation age of clay minerals associated with fault gouge using the K–Ar dating technique. Clay mineral formation is a fundamental process in the evolution of faults under the brittle regime (<<300 °C). K–Ar ages (9 fractions from 3 samples collected along a transect in the Sierra de Ambato) vary from Late Devonian to Late Triassic (~360–220 Ma). This age distribution can be explained by a long lasting brittle deformation history with a minimum age of ~360 Ma and a last clay minerals forming event at ~220 Ma. Moreover, given the progression of apparent ages decreasing from coarse to fine size fractions (~360–311 Ma for 2–1 μm grain size fraction, ~326–286 Ma for 1–0.2 μm and ~291–219 Ma of <0.2 μm), we modeled discrete deformation events at ~417 Ma (ending of the Famatinian cycle), ~317–326 Ma (end of Gondwanic orogeny), and ~194–279 Ma (Early Permian - Jurassic deformation). According to our data, the Neogene reactivation would not have affected the K–Ar system neither generated a significant clay minerals crystallization in the fault gouge, although an exhumation of more than 2 Km is recorded in this period from stratigraphic data.

1. Introduction

Stratigraphic relationships (e.g., Caelles et al., 1971; Strecker et al., 1989; Kleidert and Strecker, 2001; Mortimer et al., 2007; Carrapa et al., 2008; Bossi and Muruaga, 2009; Vazquez, 2010; Nóbile and Dávila, in prep.) as well as some low-temperature thermochronologic data (e.g., Coughlin et al., 1998; Kleinert and Strecker, 2001; Sobel and Strecker, 2003; Löbens et al., 2013; Dávila and Carter, 2013) in the transitional region between the Andean plateau (Puna) and the Sierras Pampeanas Argentine broken foreland (27–29° SL) (Fig. 1A), indicate that the main deformation and uplift would have occurred within the Cenozoic. To the south, in the Sierras de Córdoba and San Luis (or southern Argentine broken foreland, Fig. 1A), the lack of Cenozoic cooling ages together with the high recurrence of Cretaceous ages (~70–80 Ma) drove most authors to propose a low-denudation episode in the formation of the mountain belts (Jordan et al., 1989; Carignano et al., 1999; Löbens et al., 2010). Recent studies using K–Ar gouge dating technique in this region interpreted a long-lasting brittle faulting history since Carboniferous times (Löbens et al., 2010; Bense et al., 2014). They attribute the lack of Tertiary K–Ar ages to the basement cooling below illite formation temperature, indicating that exhumation and uplift driven by the Andean compression might be less significant for this region. Nevertheless, the strong differences in thermochronologic ages as well as the lack of Tertiary K–Ar ages in fault gouges might be

* Corresponding author.
E-mail address: julicaronobile@gmail.com (J.C. Nóbile).

http://dx.doi.org/10.1016/j.jsames.2015.10.008
0895-9811/

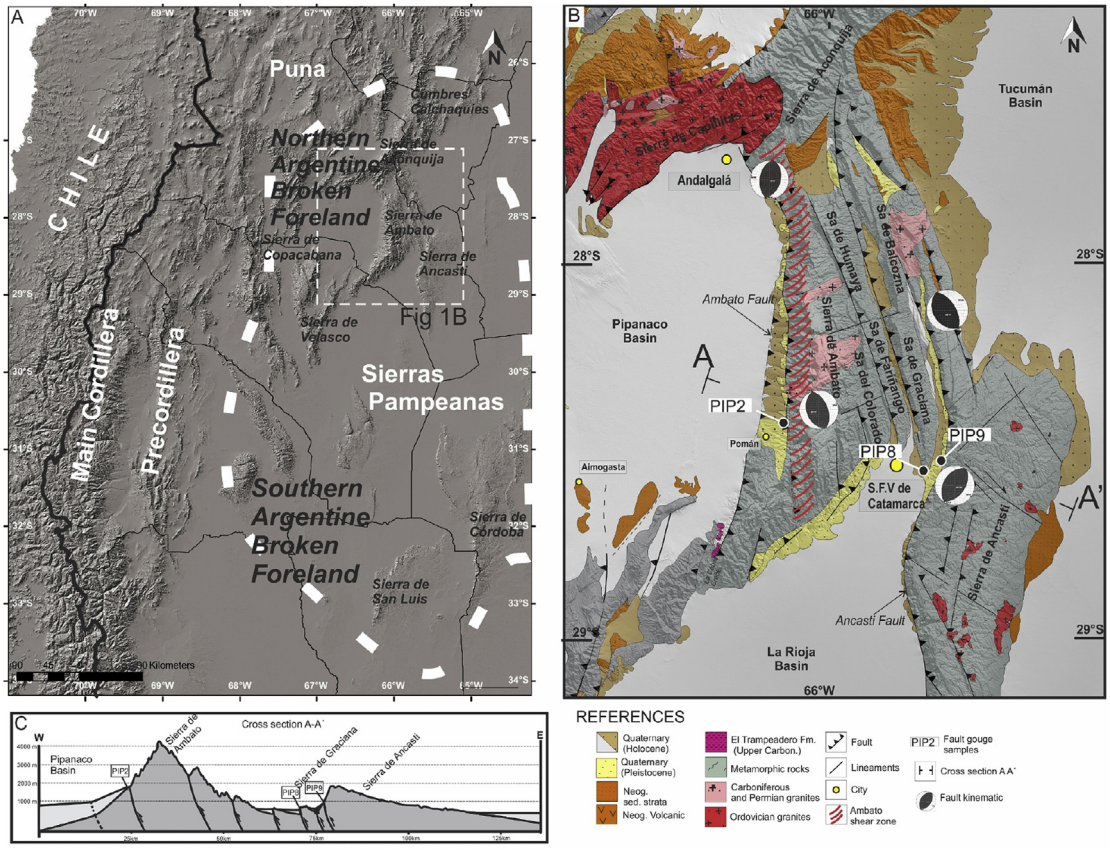

Fig. 1. A) Shaded relief map of the Argentine broken foreland, location of Sierra de Ambato and Ancasti, Sierra de Córdoba and San Luis, Sierra de Aconquija and Cumbres Calchaquíes; B) Simplified geological map of the Sierras de Ambato and Ancasti, northern Argentine broken foreland, NW Argentina. Sample locations are represented by white rectangles (name) and by black dots (location), stereonets show minor fault kinematic; C) Schematic structural cross section along line AA' (B).

alternatively indicating along strike variations in the thermal structure of the lithosphere (e.g., Dávila and Carter, 2013). The southern Argentine broken foreland (in contrast to the northern broken foreland belt) places on a flat slab subduction zone, where compression and plate coupling is high (see discussion in Dávila and Carter, 2013). The main objective of this research is to constrain and estimate the contribution of the Andean deformation to the exhumation and uplift of the northern broken foreland using the K–Ar method to date authigenic clay minerals formed in clay-rich fault gouge. We model both the obtained ages and the thermal fluctuations of the region. The selected region in the northern Argentine broken foreland shows clear evidences of Cenozoic deformation (crystalline basement thrust and progressive rotation of the synorogenic Neogene deposits) and Cenozoic low-temperature thermochronological ages. We took into account a 2-km relief for sampling (e.g., cerro El Manchao, 4550 m a.s.l.) given that new clay mineral phases within the fault gouge grow above around 50 °C (Velde et al., 1986).

2. Geological setting

The Cenozoic uplift of the Argentine broken foreland ranges, or Sierras Pampeanas, have been explained by a combination of shallow and deep processes, basement thrusting and dynamic topography, occurred since the installation of the Neogene-Present flat slab subduction regime (e.g., Isacks et al., 1982; Jordan et al., 1983; Jordan and Allmendinger, 1986; Ramos et al., 1991; Kay and Abbruzzi, 1996; Ramos et al., 2002; Dávila and Lithgow-Bertelloni, 2013). However, this region in the Argentina interior has been affected by recurrent orogenic events since the early Cambrian. These orogenies would have constructed the main mountain belts that were then reworked during subsequent deformation phases, for example, during the Andean compression (Mpodozis and Ramos, 1989).

The Sierras Pampeanas, from 27° to 34° SL (see Fig. 1A), is essentially compounded of a Lower Paleozoic crystalline basement (igneous and metamorphic) (Aceñolaza et al., 1996, 2000; Sims et al., 1998; Pankhurst et al., 1998; Rapela et al., 1998, 2007; Büttner et al., 2005; Dahlquist et al., 2006; Steenken et al., 2004, 2008; Collo et al., 2009; Verdecchia and Baldo, 2010), formed during the Early Paleozoic accretionary margin history of western Gondwana. After a long break (over 50 my, from the Silurian to Middle Devonian) in the magmatic activity of the arc, a Late Devonian to Early Carboniferous intracratonic magmatism occurred in this region, represented by A-type granites (Fig. 1B) and related to extensional tectonics (Grosse et al., 2009; Dahlquist et al., 2010; Alasino et al., 2012). The remaining Late Paleozoic stratigraphic record was dominated by alluvial-fluvial sedimentation (from glacial to semiarid environments) developed within a retroarc foreland setting, known as the Paganzo Basin (Fernandez-Seveso and Tankard, 1995). During the Mesozoic extensional settings dominated the central part of Argentina as a result of the generalized breakup and fragmentation of Pangaea/Gondwana (Uliana et al., 1989; Rossello and Mozetic, 1999; Ramos et al., 2002). Most of the Sierras Pampeanas records rifting tectonics and sedimentation during this period. Finally, with the opening of the Atlantic Ocean and westward displacement of South America (Husson et al., 2012), a net compression occurred and the Cenozoic

Andean orogeny took place. Most authors proposed that the Neogene deformation phase reused the older structures generated during the former tectonics events described above.

The study area places in the northeastern Argentine broken foreland, between 27°–29° SL, along the Sierras de Ambato and Ancasti (Fig. 1B). This region shows west-vergent, steep reverse faults that overthrust Ordovician metasedimentary basement rocks (phyllites to granulites, e.g., Caminos, 1979; Toselli et al., 1986). The thrust geometry has generated asymmetric profiles across the ranges, with steep western slopes and gentle east flanks (Fig. 1C). The metamorphic basement in mainly formed by the Ancasti Formation, with sedimentation ages between 680 and 570 Ma (Rapela et al., 2007; Murra et al., 2011) and a metamorphic episode between ~477 and 470 Ma (U–Pb geochronology on monazite grains, Larrovere et al., 2011). The igneous activity is Middle to Late Ordovician (Knüver, 1983; Toselli, 1992; Toselli et al., 1996; Pankhurst et al., 2000; Rossi et al., 2002; Rapela et al., 2005) and Devonian-early Carboniferous (Knüver, 1983; Toselli, 1983; Indri and Barber, 1987; Toselli, 1992) (Fig. 1). A ductile shear zone affecting basement rocks (Ambato shear zone, Fig. 1B) (González Bonorino, 1953) crops out in the NW part of Sierra de Ambato. This deformation was constrained in the early Cambrian-Ordovician (Larroverre et al., 2008) through intrusion relationships. The oldest exposed sedimentary unit is a glacial Carboniferous succession (Trampeadero Formation, Fig. 2A, González Díaz, 1970; Gutierrez and Barreda, 2006), which rests on the crystalline basement and is in turn covered by Quaternary deposits. Cretaceous sediments are absent in the Sierra de Ambato, although thin strata (~90 m), crops out further south (approx. 100 km) in La Rioja creek (Tauber, 2002), and toward north in the Cumbres Calchaquíes (Grier et al., 1991; González, 2000).

On the gentle eastern flank of the Sierras de Aconquija and Ambato (Fig. 1B), thick alluvial Neogene strata (ca. 2000 m, Aconquija Formation, Fig. 2B and C; González Bonorino, 1950; Nasif et al., 2007) lap onto a flattened surface developed on crystalline basement (Pampean planation surface or peneplain, Jordan et al., 1989). However, geophysical data from nearby areas (e.g., Fisher et al., 2002; Cristallini et al., 2004; Mortimer et al., 2007; Dávila et al., 2012) have reported ~3.5 km of Cenozoic strata. Quaternary conglomerates (~1.8 Ma, Duarte, 1997) lay unconformably on Neogene (Fig. 2D), representing the first records of intermontane sedimentation within the Sierra de Ambato and Sierra de Ancasti. The stratigraphic relationships and new ages (Nóbile and Davila, in prep.) suggest the thrusting, tilting and uplift of the thrust sheets would have occurred after 9 Ma.

3. Theoretical framework

The K–Ar dating of authigenic clay minerals phases formed in fault gouge can provide an accurate method to constrain shallow faults and/or to determine different periods of motion along a fault (e.g., Lyons and Snellenburg, 1971; Kralik et al., 1987; Ylagan et al., 2002; van der Pluijm et al., 2001, 2006; Hayman, 2006; Haines and van der Pluijm, 2008; Löbens et al., 2010; Bense et al., 2014). Fault gouges mainly consist of few large rock fragments isolated in a matrix rich in clay minerals. They are usually found in faults that have been active at shallow crust (<4 km, Sibson, 1977; Passchier and Trouw, 2005) (Fig. 3) under a cataclastic regime above a certain stress level (brittle regime, <300 °C) during repeated fault movement. The matrix consists of newly grow clay minerals formed due to hydration reactions (usually illite and interestratified illite/smectite; Zwingmann and Mancktelow, 2004) and can contain fragmental fine-grained phyllosilicates inherited from the host rock. Consequently, radiometric dating of authigenic clay minerals should contemplate the possible presence of detrital material, producing mixed ages (Pevear, 1992; Grathoff et al., 2001), but also the presence of authigenic mineral assemblages growing along the protracted history of the fault and under multiple deformation mechanisms (e.g., Hayman, 2006, Fig. 3). In order to identify these mixtures of phases originated in different events, a physical separation of different grain size fractions should be performed (Haines and van der Pluijm, 2010) and a mineralogical characterization of

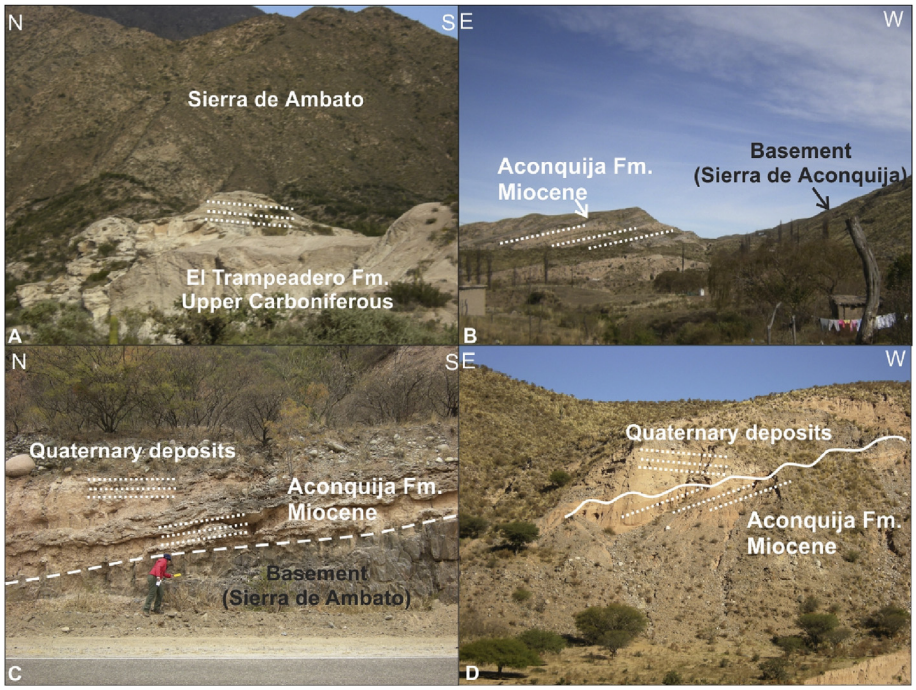

Fig. 2. A) El Trampeadero Formation (Upper Carboniferous) at La Cébila creek; B) Stratigraphic relation between Aconquija Formation (Miocene) and basement (Pampean peneplain) in Sierra de Aconquija, C) and Sierra de Ambato; D) and Quaternary conglomerates lapping unconformably Miocene strata. Notice that the Miocene units rest subparallel on the basement peneplain (B and C).

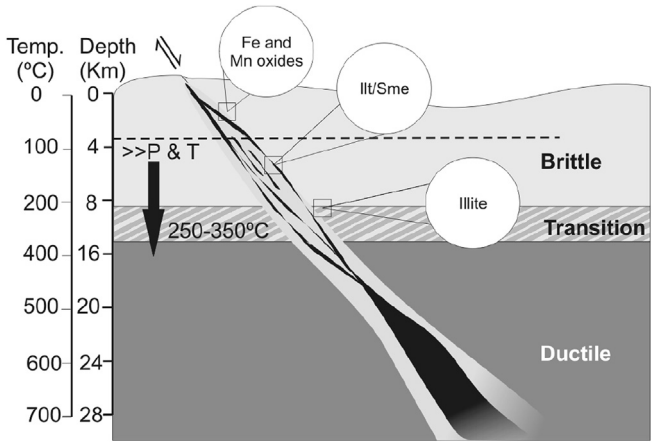

Fig. 3. Conceptual model of a major fault zone (modified from Sibson, 1977) and location of different phases of gouge clay minerals at different depth and Fe and Mn-oxides at superficial levels (Hayman, 2006). The vertical scale is given considering a geothermal gradient of 25 °C/Km. Ilt/Sme: interestratified illite/smectite.

each fraction must be achieved.

4. Methods

4.1. Sampling and sample preparation

We analyzed three fault zones (PIP2, PIP8 and PIP9) along the steep western flanks of the Sierra de Ambato, Sierra de Humaya/Farignano, Sierra de Graciana and Sierra de Ancasti (Fig. 1B). They are >100 m thick and orientated NNW (~330°) and dipping 30°–45°E. The fault rocks show a gradual transition from the non-deformed basement to the damage zone, mainly gouges. We observed iron patinas and calcite across the faults. Slickenside kinematic indicators (Fig. 4 E–F) reveals reverse kinematics (González Bonorino, 1950 and Fig. 1 B). Our kinematics analysis on the different fault planes matches with crustal focal mechanism studies, which evidenced shortening events with a minor strike-slip component (Alvarado and Ramos, 2011). We collected ~1 kg of fault gouges from each damage zone (Fig. 4). While PIP2 was collected in the Ambato thrust (Fig. 4 A–B) affecting phyllites, the PIP8 and PIP9 host rocks, in the Sierra de Graciana and Ancasti (Fig. 1B), are migmatites and gneisses (Fig. 4 C–D).

We disaggregated the gouge samples and then removed carbonates and organic materials following the recommendations of Moore and Reynolds (1997). In order to isolate fine-grained clays with varying proportions of authigenic clays, we separated three size fractions (2–1 μm, 1–0.2 μm and <0.2 μm) using a centrifuge. The grain size distributions were established for each fraction through a Laser Particle Analyzer Horiba LA-950 (Fig. 5). The precision (repeatability) of the analyzer has been tested using a synthetic mixture of glass particles (NIST traceable standard polydisperse particles PS202/3-30 m and PS215/10–100 mm in Whitehouse Scientific®). For both analyses (PS202, PS215 and $n = 6$, $n = 5$) average (D50) was within 3% of nominal value and percentiles D10 and D90 not fit within 5% of the nominal value for the standards. Finally, we prepared oriented aggregates for each sample to be analyzed using XRD.

4.2. Analytical methods and procedures

In order to identify and semi-quantify the different K-bearing phases present in each separated fraction the oriented aggregates were analyzed using PANalytical X'Pert PRO diffractometer at the "Facultad de Ciencias Químicas" (Universidad Nacional de Córdoba, Argentina) using Cu radiation from 4 to 30°2θ, with a step size of 1°2θ/min and diffractograms were obtained from air-dried (AD), ethylene-glycol solvated (EG; 24 h), and heated (at 500 °C for 4 h) slides. Clay–mineral phases were semi-quantified using MIF factors and the recommendations of Moore and Reynolds (1997).

The Kübler index (KI; Kübler, 1968; Kisch, 1991) allows estimating the temperature conditions during the clay gouge formation and the intensity of illite growth processes. The KI was measured in the fine-grained white mica (001) reflection in both AD and EG oriented clay mineral aggregates, and KI_{CIS} values (CIS: Crystallinity Index Standard, Wart and Rice, 1994) were established from the regression equations for the diffractometer employed.

To quantify the different phases of clay minerals, we performed a decomposition of reflections in the angular interval between 5 and 11° 2θ EG diagrams using the ProFit 1.0c software (cf. Lanson and Velde, 1992; Lanson, 1997), distinguishing illite from R3-ordered and R0-disordered mixed layer illite/smectite (Meunier and Velde, 2004).

K/Ar clay minerals ages were determined at the Geoscience Centre of the University of Göttingen for each fraction by the following procedure: The argon isotopic composition was measured in a Pyrex glass extraction and purification line coupled to an ARGUS VI multi-collector noble gas mass spectrometer operating in static mode. The amount of radiogenic ^{40}Ar was determined by isotope dilution method using a highly enriched ^{38}Ar spike from Schumacher, Bern (Schumacher, 1975). The spike was calibrated against the biotite standard HD-B1 (Fuhrmann et al., 1987). The age calculations were based on the constants recommended by the IUGS quoted in Steiger and Jäger (1977). Potassium was determined in duplicate using a BWB XP flame photometer. The samples were dissolved in a mixture of HF and HNO_3 according to the technique of Heinrichs and Herrmann (1990). The analytical error for the K/Ar age calculations is given on a 95% confidence level (2σ).

Based on the ages and relative percentages of clay mineral phases of the three different grain-size fractions in each sample, we performed a linear correlation to obtain extrapolated ages (Solum et al., 2005; van der Pluijm et al., 2006; Haines and van der Pluijm, 2008). Moreover, we modeled the corrected ages with Modelage 1.0 (Szczerba and Środoń, 2009). This program considers illite/illite-smectite ratio as proxies for the ratio of detrital and diagenetic components and calculates the end-member ages and the $^{40}K_{detrital}/^{40}K_{diagenetic}$ ratio using genetic algorithms that contemplate the potassium content in these end-member clay minerals (Szczerba and Środoń, 2009). For each sample we determined two extrapolated ages: Modeled ages 1 (MA1) and 2 (MA2).

4.3. Basement thermal history

We modeled the burial-exhumation history for one of the samples using PetroMod 1D Express Basin Modeling (from IES GmbH, Schlumberger). The modeling included the reconstruction of the depositional and erosional intervals as well as the temperature history (paleo-heat flow variations). PetroMod runs numerical simulations considering input parameters such as stratigraphic intervals (initial thickness, eroded thickness, lithology and age), paleo-water depth (PWD), seawater interface temperature (SWIT), and heat flow (HF) values.

5. Results

5.1. Characterization and semiquantification of the clay mineral fractions

The grain size distributions established for each fraction are

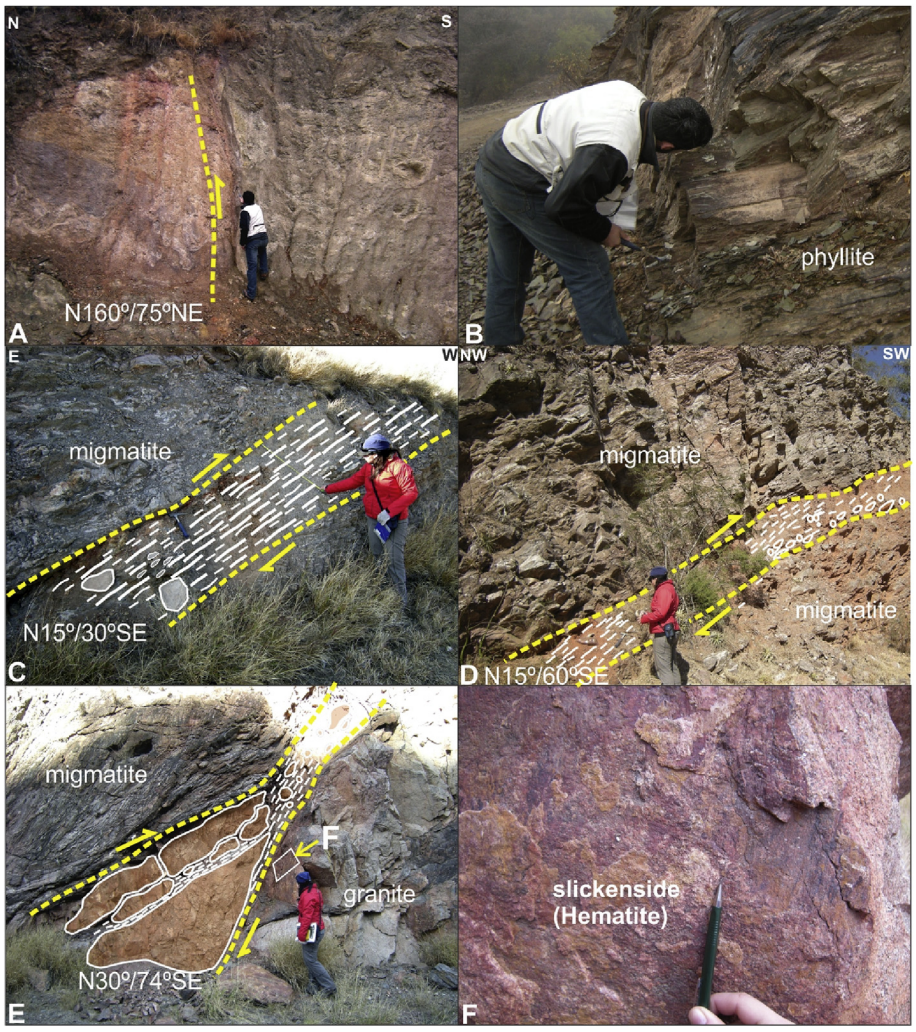

Fig. 4. Gouge-bearing fault zones from the study area: A) fault zone at sample PIP2 and gouge detail and B) host rock at Ambato fault (sample PIP2); C) fault zone for sample PIP8 (Sierra de Graciana); D) fault zone for sample PIP9 (Sierra de Ancasti); E) fault zone in Sierra de Ambato with detail of slickenside (F).

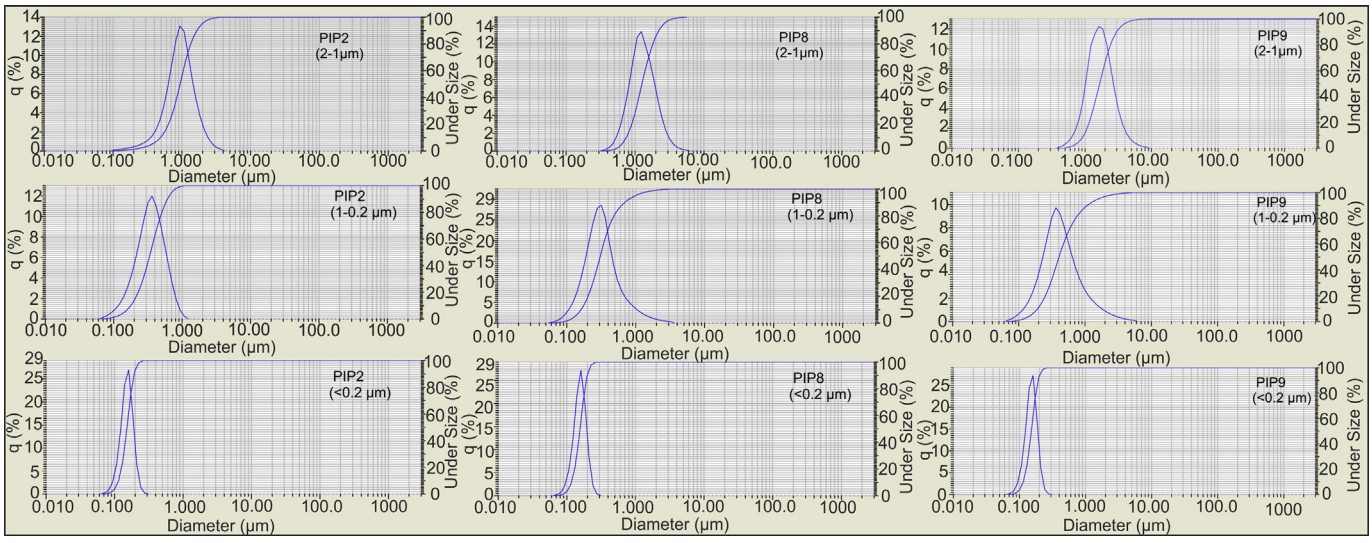

Fig. 5. Grain size frequency + cumulative (undersize) curves for each fraction using a Laser Particle Analyzer Horiba LA-950.

shown in Fig. 5. The clay mineral phases identified through XRD analyses for the nine sub-samples (from the three fault gouge samples) are shown in Table 1 and Fig. 6.

Sample PIP2 has illite, chlorite as the major clay mineral components with minor traces of quartz and feldspar. Decomposition in the 5°–11° 2θ angular interval of XRD patterns shows that the coarser fraction is dominated by illite, with R3 in the finest fraction. No R0 I/S was identified in this sample. Major clay mineral components of PIP8 are illite, I/S and kaolinite, with quartz and K-feldspar as minor components. No chlorite was identified. Decomposition shows that illite and R3 are present in all fractions, with R0 in the two finest fractions. PIP9 has illite, I/S (R3) and chlorite as major clay mineral components, with presence of R0 in the coarser fraction. KI_{CIS} values for the nine fractions range from 0.46 to 1.45 Δ°2θ and are higher as the grain size decreases (Table 1). These values are typical of the diagenetic zone to anchizone (<200 °C).

The sample PIP2 is affecting a phyllite, and then illite and I/S contribution from host rock should be contemplated in the K–Ar ages results. According to Verdecchia et al. (2011) phyllite rocks from the southern Sierra de Ambato (in La Cébila creek, Fig. 1B) have abundant illite, kaolinite, vermiculite, smectite and chlorite and KI_{CIS} values ranging from 0.17 to 0.46 Δ°2θ. For low-grade metamorphic host rocks, with illite and chlorite, it is difficult to differentiate newly grown clay minerals from host phyllosilicates. In samples PIP8 and PIP9, which involve high-grade metamorphic basement rocks, the obtained KI_{CIS} values (ranging from 0.5 to 1.5 Δ°2θ, Table 1) allow discarding the presence of inherited muscovite (with KI_{CIS} ca. 0.060 Δ°2θ, Wart and Rice, 1994). Moreover, given the presence of K-feldspar in the coarsest fraction of PIP2, the age obtained for this fraction should contemplate the contribution of inherited material from basement.

5.2. K–Ar ages

Potassium (K_2O) concentration ranges from 2.45 to 6.18% (Table 2). The results show K/Ar ages (9 grain-size fractions) ranging from Late Devonian to Late Triassic (~360–220 Ma, Table 2). The K–Ar ages from sample PIP2 are 328.1 ± 6.1 Ma for 2–1 μm fraction, 325.6 ± 4.8 Ma for 1–0.2 μm fraction, and 291.2 ± 3.9 Ma for <0.2 μm fraction. The sample PIP2 shows an age gap between the 2–1 μm fraction and the smallest fractions but overlapping ages, within the error, between 1 and 0.2 μm and <0.2 μm fractions. K–Ar ages from samples PIP8 and PIP9 do not overlap in any fractions. Sample PIP8 yielded K–Ar ages of 358.5 ± 6.9 Ma for 2–1 μm fraction, 304.4 ± 6.9 Ma for 1–0.2 μm fraction and 285.6 ± 3.1 Ma for <0.2 μm fraction. Finally, the K–Ar ages from sample PIP9 are 311.3 ± 4.1 Ma for 2–1 μm fraction, 280.8 ± 3.4 Ma for 1–0.2 μm fraction and 219.8 ± 6.1 Ma for <0.2 μm fraction. In all the cases the youngest ages correspond to the <0.2 μm grain size.

For clays, the proposed closure temperature interval of the K–Ar system is between ~260 and 350 °C (Purdy and Jäger, 1976; Hunziker et al., 1986; Wemmer and Ahrendt, 1997). Kübler indexes determined for our samples confirm temperatures below ~200 °C, which indicates that a loss of argon due to high temperature conditions is unlikely. However, argon loss by diffusion related with the small grain size of the clay minerals and time should not be ruled out.

Given the presence of K-feldespar in the coarsest fraction of PIP2 it was excluded from the age-% detrital component model (see Fig. 7). From the linear correlation between the three K–Ar ages and the percentage of clay minerals phases we obtained extrapolated end-members ages with a high correlation coefficient ($R^2 > 0.93$, Fig. 6): the lower intercept of the regression line at 100% mixed-layer illite/smectite phases (MA1) is calculated as ~271.5 Ma for sample PIP2, ~276.8 Ma for sample PIP8 and ~194.4 Ma for sample PIP9. The upper intercept at 100% illite (MA2) gives ages of 325.6 Ma for PIP2, 416.8 Ma for PIP8 and 316.7 Ma for PIP9. Comparable results were obtained using Modelage software. Modeled brittle deformation events were established at 236.7 ± 22.4 Ma and 325.6 ± 0.1 Ma for sample PIP2; 278.7 ± 0.2 Ma and 416 ± 0.1 Ma for sample PIP8 and 198.2 ± 0.4 Ma and 316.9 ± 1.0 Ma for sample PIP9 (Table 3).

6. Discussion

Our absolute ages obtained by the K–Ar dating on the fault gouge across the northern Argentine broken foreland in the Ambato region are comparable with those obtained by Bense et al. (2014), as is shown in Fig. 8. These authors conclude, on the base of a set of non-modeled K–Ar ages, that a long lasting brittle deformation history would have occurred in the Sierras de Córdoba and San Luis from the Carboniferous to the Early Cretaceous. However, the rejuvenation of K–Ar ages with the decreasing grain size constitutes a strong evidence of mixing between different clay mineral populations generated at different times. We suggest that modeling of K–Ar ages should be calculated in order to discriminate likely isolated deformation events from an apparent long lasting history of deformation. This might also allow correlating individual deformation events with the sedimentation and exhumation episodes recorded in the region. The overlapping K–Ar ages from two fractions of one sample (Nogolí samples) reported by Bense et al. (2014), argues in favor of the existence of discrete events in the southern Argentine broken foreland.

From the extrapolated and modeled ages we have established two discrete events represented by MA2 (100% illite) ages at ~417 Ma, ~317–326 Ma, and younger events represented by MA1

Table 1
Results of X-ray diffraction analyses from the sample material fractions and illite crystallinity index.

Sample	Fraction [μm]	Lat Lon	Mineralogy [%]							Clay mineral phases [%]				KI*
			Ilt	Chl	I/S	Kln	Qtz	Pl	Kfs	Illite	R3	R1	R0	[Δ°2θ]
PIP2	2–1	28.34°S	86	14	–	–	–	X	X	100	0	–	–	0.46
	1–0.2	66.13°W	95	5	–	–	X	–	–	100	0	–	–	0.46
	<0.2	–	96	4	–	–	–	–	–	36	64	–	–	0.80
PIP8	2–1	28.48°S	82	–	–	18	X	–	✓	55	45	–	–	0.50
	1–0.2	65.67°W	66	–	6	28	X	–	–	27	65	–	8	1.45
	<0.2	–	47	–	28	25	–	–	–	2	48	–	50	0.80
PIP9	2–1	28.47°S	85	5	11	–	–	–	–	86	4	–	10	0.54
	1–0.2	65.64°W	90	10	✓	–	–	–	–	81	19	–	–	0.60
	<0.2	–	88	12	✓	–	–	–	–	20	80	–	–	0.67

Notes: Ilt, Illite, Chl, Chlorite, Kln, Kaolinite, Qtz, Quartz, Pl, plagioclase, Kfs, K-feldspar, I/S, interestratified illite -smectite (R3, R1 and R0-ordered), KI* converted to CIS scale: y = 1.1162 * x + 0.0571; X minor components; ✓ traces.

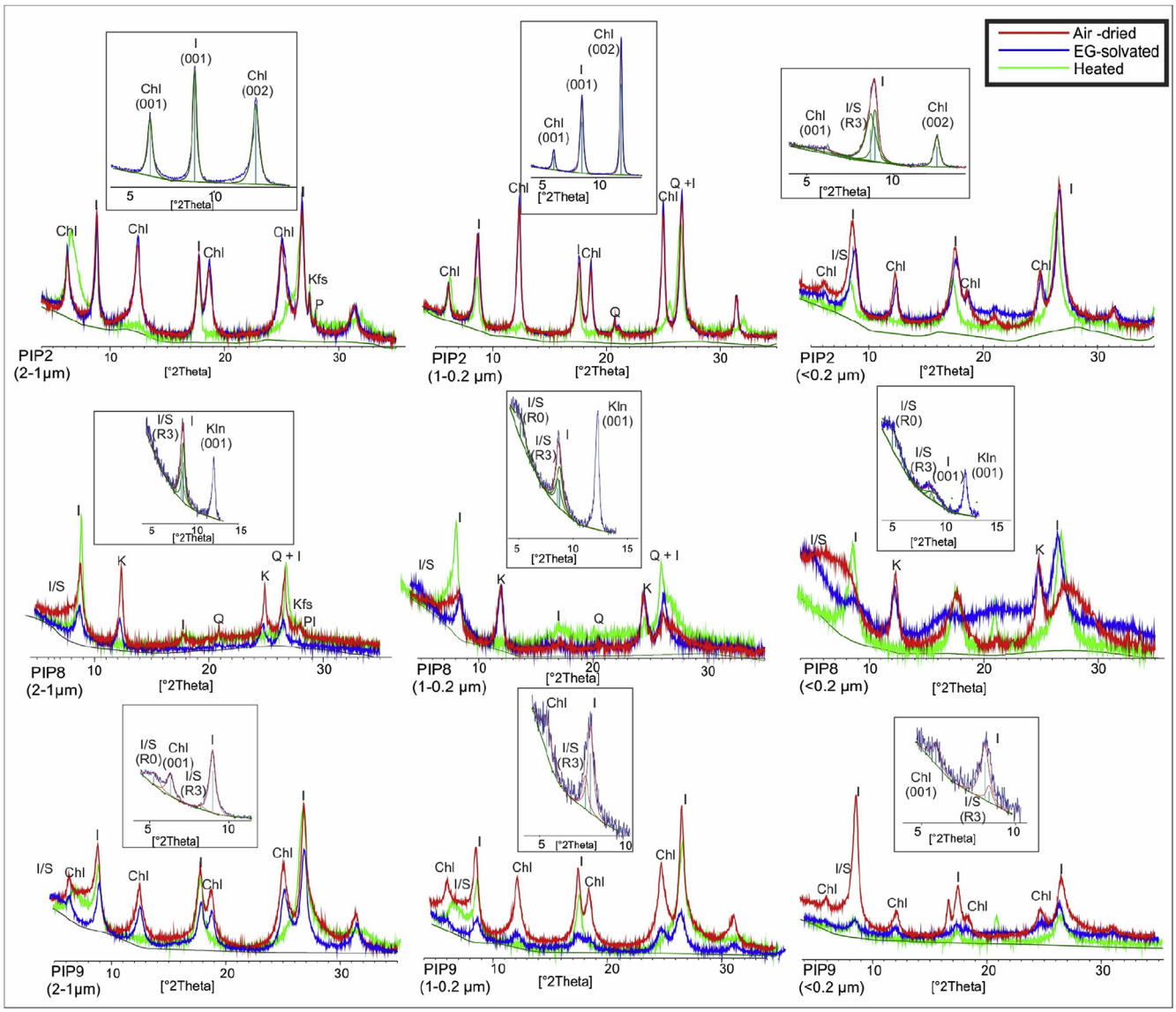

Fig. 6. XRD patterns obtained for each fault gouge samples and grain-size fraction (2–1 μm, 1–0.2 μm, <0.2 μm). Inset box the relative proportions of interestratified illite/smectite phases established from decomposition in the 5°–11° 2θ angular interval of ethinglycol solvated (EG) XRD patterns using the Profit 1.0c software.

(0% illite) ages between ~194 and 279 Ma, which likely record the cooling of the host rock from epizonal and anquizonal conditions. Particularly, MA2 corrected age for the sample PIP8 at ~417 Ma (Silurian-Devonian boundary) could be attributed to the end of the Famatinian cycle after the collision of the Precordillera terrane (Astini and Dávila, 2004, Fig. 9). Although the main deformation phase of the Famatinian orogeny would have occurred between ~480 and 465 Ma (Ordovician), there are evidences of later

Table 2
K–Ar ages of different clay minerals fractions.

Sample	Grain size [μm]	K–Ar data				
		K_2O [Wt. %]	$^{40}Ar^a$ [nl/g] STP	$^{40}Ar^a$ [%]	Age [Ma]	±2σ-error [Ma]
PIP2	2–1	4.96	57.59	98.09	328.1	6.1
	1–0.2	6.1	70.19	99.35	325.6	4.8
	<0.2	6.18	62.99	97.7	291.2	3.9
PIP8	2–1	2.83	36.19	92.38	358.5	6.9
	1–0.2	3.00	32.03	93.46	304.4	6.5
	<0.2	2.45	24.41	93.4	285.6	3.1
PIP9	2–1	5.06	55.39	97.94	311.3	4.1
	1–0.2	5.83	57.11	96.59	280.8	3.4
	<0.2	3.06	23.04	92.37	219.8	6.1

[a] Radiogenic argon.

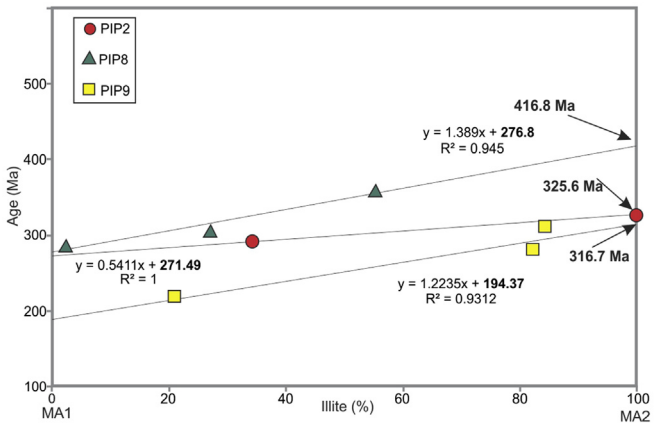

Fig. 7. Linear extrapolation of K–Ar end member ages from each sample; see Table 1 for % of illite and Table 2 for K–Ar dating of different size fractions. MA1, modeled age 1; MA2, modeled age 2.

deformation events during the Silurian-Devonian in basement rocks from the northwestern broken foreland (~402 Ma Sm–Nd garnet age from the TIPA shear zone, Höckenreiner et al., 2003, Fig. 1A) and more than 400 km southward in the Sierras de Córdoba (~441–414 Ma K–Ar muscovite dating; Steenken et al., 2010, Fig. 1A). It is important to note that as muscovite closure temperatures are slightly higher (~300–420 °C, Reiners et al., 2005; Harrison et al., 2009) than those proposed for the illite formation (until ~300 °C, Hunziker et al., 1986), the cooling ages are comparable with the PIP8 authigenic illite age. The MA2 ages for PIP2 and PIP9 are ~317 and ~326 Ma (early-middle Carboniferous), which well correlates with other low-temperature cooling ages reported in the northeastern broken foreland (Fig. 9). U–Th/He zircon data (ZHe; closure temperature ~200–160 °C; Reiners et al., 2005) from the Aconquija/Cumbres Calchaquíes basement yield ages between ~340 and ~309 Ma (Löbens et al., 2013, Fig. 9). These cooling ages could be related with the exhumation associated to the Early Carboniferous mountain building and glacial valley formation (Astini, 2009; Isbell et al., 2012).

Extrapolated MA1 ages are ~194–198 and 237–279 Ma (Fig. 7). Bense et al. (2014) reported similar cooling ages using the same method on fault rocks from the Sierras de Córdoba and San Luis in the southern broken foreland emphasizing the regional character of these events. Middle Permian-Lower Triassic ages from PIP2 and PIP8 are interpreted as result of the Gondwanide/San Rafaelic orogeny (cf., Mpodozis and Ramos, 1989; Llambias et al., 2003) that exhumed the Paganzo basin (Fig. 9). The Lower Jurassic age obtained for PIP9 is likely recording an extensional reactivation of older structures.

From the comparison between non-modeled and modeled ages it is clear that oldest and youngest episodes recorded in the fault gouges are masked by the initial K–Ar mixing ages and discrete episodes could be overlooked if modeled ages are not considered in the analysis. Moreover, our results and K–Ar age modeling show that the fault ages vary across the studied region. Considering the ranges of thermal stability for the different clay mineral phases and the modeled K–Ar ages (MA1 and MA2), a time-temperature path for the samples can be modeled (Fig. 10). We considered illite formation temperatures between 100 and 300 °C (cf. Hunziker et al., 1986; Merriman and Peacor, 1999; Vrolijk and van der Pluijm,

Table 3
Resume table showing corrected and extrapoled ages for PIP2, PIP8 and PIP9.

Sample	Linear extrapolation		Modelage 1.0 extrapolation		FIT
	M2 (100% Illite)[Ma]	M1 (100% Ilt/Sme) [Ma]	M2 (100% Illite) [Ma]	M1 (100% Ilt/Sme) [Ma]	
PIP2	325.6	271.5	325.6 ± 0.1	236.7 ± 22.4	999.76
PIP8	416.8	276.8	416 ± 0.1	278.7 ± 0.2	59.27
PIP9	316.7	194.4	316.9 ± 0.1	198.2 ± 1.0	31.77

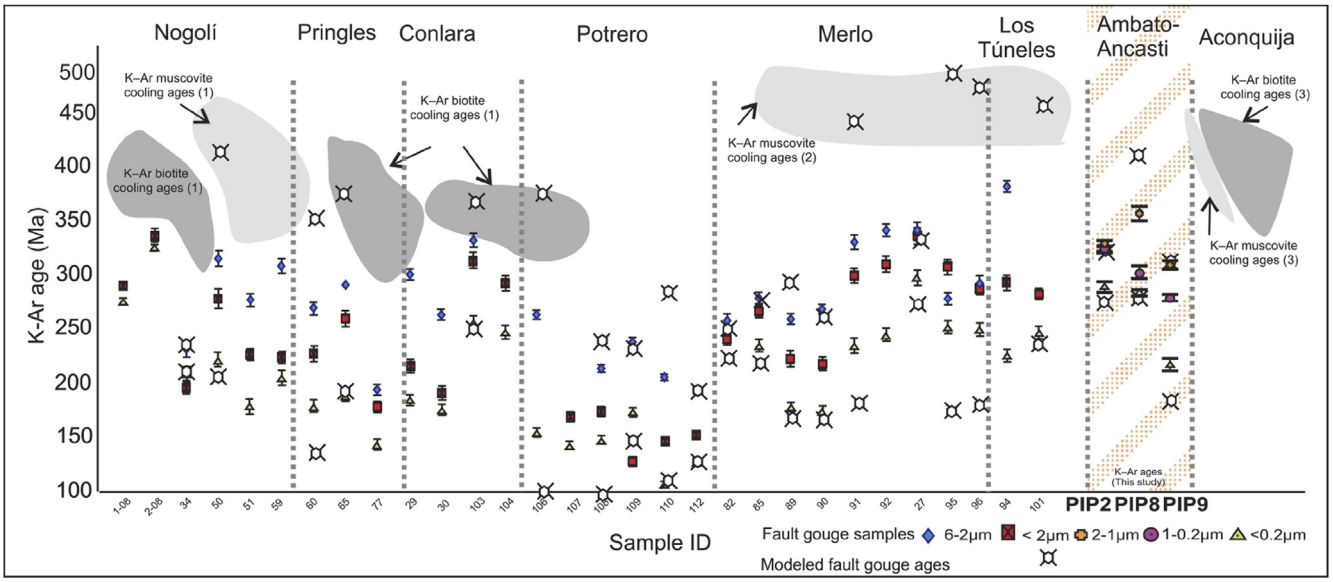

Fig. 8. Compilation of K–Ar fault gouge ages (different grain size fractions) from Sierras Pampeanas of Córdoba and San Luis (Bense et al., 2014) and from Sierra de Ambato and Ancasti (this work). Dark areas show K–Ar muscovite and biotite cooling ages taken from Steenken et al., 2008 (1), 2010 (2) and Löbens et al., 2013 (3).

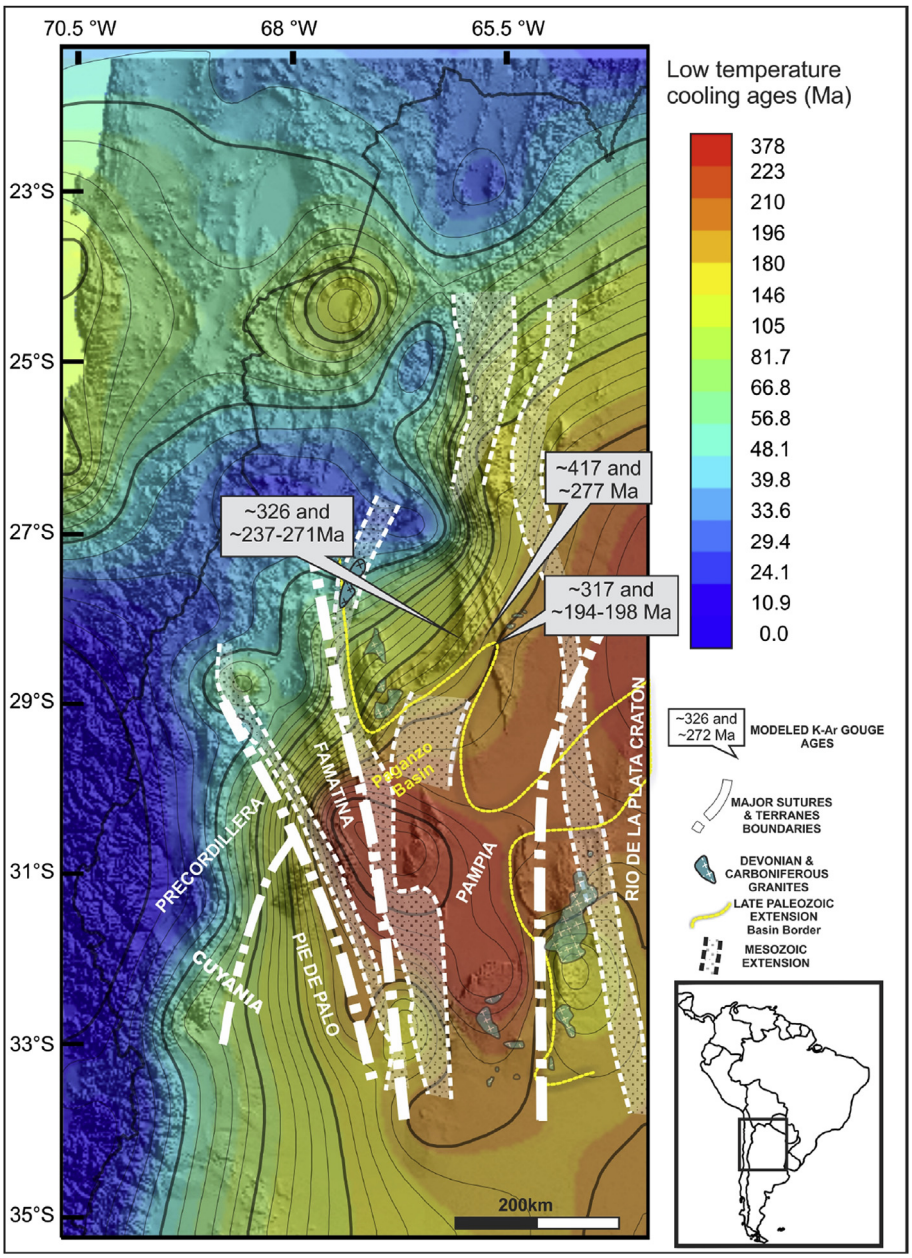

Fig. 9. Contour map of published low temperature thermochronology cooling ages along South central Andes (after Dávila and Carter, 2013) with major discontinuities (after Ramos et al., 2002): white dash-dotted line shows main sutures and terrane boundaries; yellow dotted line show the late Paleozoic Paganzo basin border; dotted shaded areas show the location of major rift systems of Triassic-early Jurassic and early Cretaceous age, and green shaded areas the locations of Devonian and Carboniferous granites. (For interpretation of the references to colour in this figure legend, the reader is referred to the web version of this article.)

1999) and between 65 and 220 °C for the formation of high ordering (R3) mixed-layer illite/smectite (Velde et al., 1986; Środoń, 2007).

Fig. 10 shows a relatively simple temperature-time path considering the calculated ages and formation temperatures for each fraction. In sample PIP8 a rapid cooling history from Ordovician to Silurian-Devonian and a slowly cooling from Devonian to present-day are observed. Sample PIP2 shows a rapid cooling from Carboniferous to Permian and depict a slowly cooling from Permian to present-day, whereas sample PIP9 depict a slowly cooling from Ordovician to present-day. The conversion of this temperature-time path to a depth-time path requires knowing the changes of the thermal state in the region along the history. This was achieved for the Sierra de Ambato (sample PIP2) using the PetroMod software (see 4.3 for further details) and considering heat flow variations (according to the present day analogues for different tectonic settings interpreted for the region along the geological history) and the sedimentary records. The latter is very important as exhumation or burial episodes strongly affect the results. Fig. 11 shows the model result and a hypothetical path for the sample PIP2 within the upper crust (uppermost 12 km). Heat flows were estimated considering the different geotectonic context for the region from Paleozoic to present (cf. Gutscher et al., 2000; Collo et al., 2011; Jaupart and Mareschal, 2007; Furlong and Chapman, 2013). The sedimentation stages for the northern broken foreland were considered from preserved stratigraphic records (González Díaz, 1970; Gutierrez and Barreda, 2006; Mamani et al., 2002; Fisher et al., 2002; Sobel and Strecker, 2003; Dávila et al., 2012). The

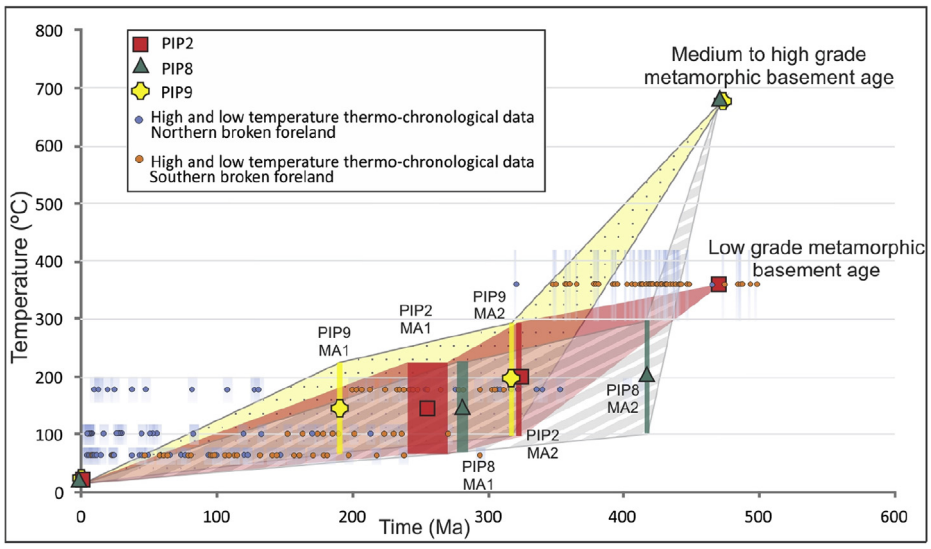

Fig. 10. Time-temperature paths considering thermal stability (shaded areas) for different phases of clay minerals in each sample (PIP2, PIP8 and PIP9) and modeled K–Ar clay minerals fault-gouge discrete ages (rectangle, triangle and cross). Temperatures between 100 and 300 °C were considered for illite formation (Hunziker et al., 1986; Merriman and Peacor, 1999; Vrolijk and van der Pluijm, 1999) and temperatures between 65 and 220 °C, were considered for the high ordering (R3) mixed-layer illite/smectite formation (Velde et al., 1986; Środoń, 2007). Compilation of high- and low temperature thermochronological data from the Argentine broken foreland (orange circles indicate ages from southern broken foreland and light blue circles from northern broken foreland). The K–Ar Muscovite data were extracted from Steenken et al. (2008, 2010) and Löbens et al. (2013); ZHe and AHe data were extracted from Löbens et al. (2010, 2013), Bense et al. (2013), AFT data from Löbens et al. (2013), Bense et al. (2013). (For interpretation of the references to colour in this figure legend, the reader is referred to the web version of this article.)

two discrete deformational (exhumation) events at ~326 Ma (Fig. 11A) and ~237–272 Ma (Fig. 11B) are used to constrain the path, according the modeled K–Ar ages. The model shows more than 2.5 km of exhumation during the Carboniferous (Fig. 11A) in accordance to geochronological data from the TIPA shear zone (Hockenreiner et al., 2003). Assuming that exhumation is proportional to uplift, this exhumation might have favored the mountain building and conditions to develop the glacial valleys reported in the region and represented by the tillites of the Trampeadero Formation (~320–280 Ma, González Díaz, 1970, Gutierrez and Barreda, 2006). The second exhumation episode (Fig. 11B) is constrained to the Permian–Middle Triassic and would have generated a lower relief, likely associated with the San Rafael orogenic phase (Llambias et al., 2003). After this event, the model shows a flat path almost until the Neogene. A late Cenozoic exhumation following a Neogene sedimentation episode is interpreted from geological relationships (Dávila et al., 2012, Fig. 11C). The clockwise rotation and exhumation of the Miocene Aconquija Fm. (~2 Km thick) support our interpretations. It is important to note that as a consequence of the very low heat flow reported for the Argentine broken foreland during the Neogene (Collo et al., 2011; Dávila and Carter, 2013) the crustal thermal gradient would have been <17 °C and consequently at ~1–3 km the temperature would have been <50 °C, inhibiting the growth of newly formed Tertiary gouge clay minerals (Fig. 11C).

On the base of our results, models and interpretations, the lack of Cenozoic K–Ar ages in fault gouges in the northern Argentine broken foreland might be interpreted as a consequence of the low geothermal gradient instead of a low exhumation. The deep Neogene Bermejo and Vinchina basins located immediately to the west (>7 km thick) show K–Ar ages in clay minerals from sedimentary units older than the sedimentation age. This indicates unsuitable thermal conditions to form the authigenesis clay minerals (Collo et al., 2011, 2015), in agreement with very low heat flows.

From the analysis and the modeled fault gouge ages in this study, as well as the data analyzed by Bense et al. (2013) (Fig. 8), it is clear that each fault record a particular deformational history that together allow us to interpret the evolution of the region. This is consistent with a complex history of reactivation of individual faults within the same region. The Paleozoic deformation history interpreted for the Sierras de Ambato and Ancasti from the gouge ages is similar to that proposed for other regions located to the south, with exhumation–deformation episodes related to different Paleozoic–Mesozoic orogenic phases, preserved at depths and exhumed during the Andean deformation. However, in the case of the northern region, the modeled age at ~417 Ma (Silurian-Devonian boundary) allows inferring an older deformational episode than those recorded by other authors for the southern broken foreland. Moreover, our interpretation for the Andean evolution also differs. The thermal modeling suggests a Neogene burial depth of about 3 km under a low thermal gradient (25 mW/m^2), followed by an exhumation of over ~3–7 km (thickness of the exhumed basin plus thickness of the basement substrate of the Neogene basin exhumed in the Sierra de Ambato). Further north, Löbens et al. (2013) proposed a similar exhumation of about 8 km since 9 Ma for the Sierra Aconquija, assuming a geothermal gradient between 20 and 26 °C/km. To the south, the lack of Cenozoic cooling ages in different thermochronometers, as well as K–Ar fault gouge ages, led to propose a low exhumation stage (Löbens et al., 2010; Bense et al., 2014). However, considering that the Sierras de Córdoba and San Luis are currently located in the flat-slab region, low heat flow conditions similar than those inferred to the north could explain the presence of significant exhumation with no reset of the isotopic systems. The differences between the two regions could be attributed to a more important Cenozoic burial towards the north, where the low-temperature thermocronological systems would have been reset during the late Cenozoic (after 9 Ma?; Fig. 8). To the south, the poor burial (~800 m, Astini et al., 2014) together with a low temperature regime would avoid the thermochronologic resetting (Dávila and Carter, 2013), preserving older cooling ages (>50 Ma).

7. Conclusions

From XRD and K–Ar analyses three main clay mineral growth episodes are recognized at ~417 Ma, ~316–326 Ma, ~237–278 Ma and 198 Ma in the northern Argentine broken foreland, indicating

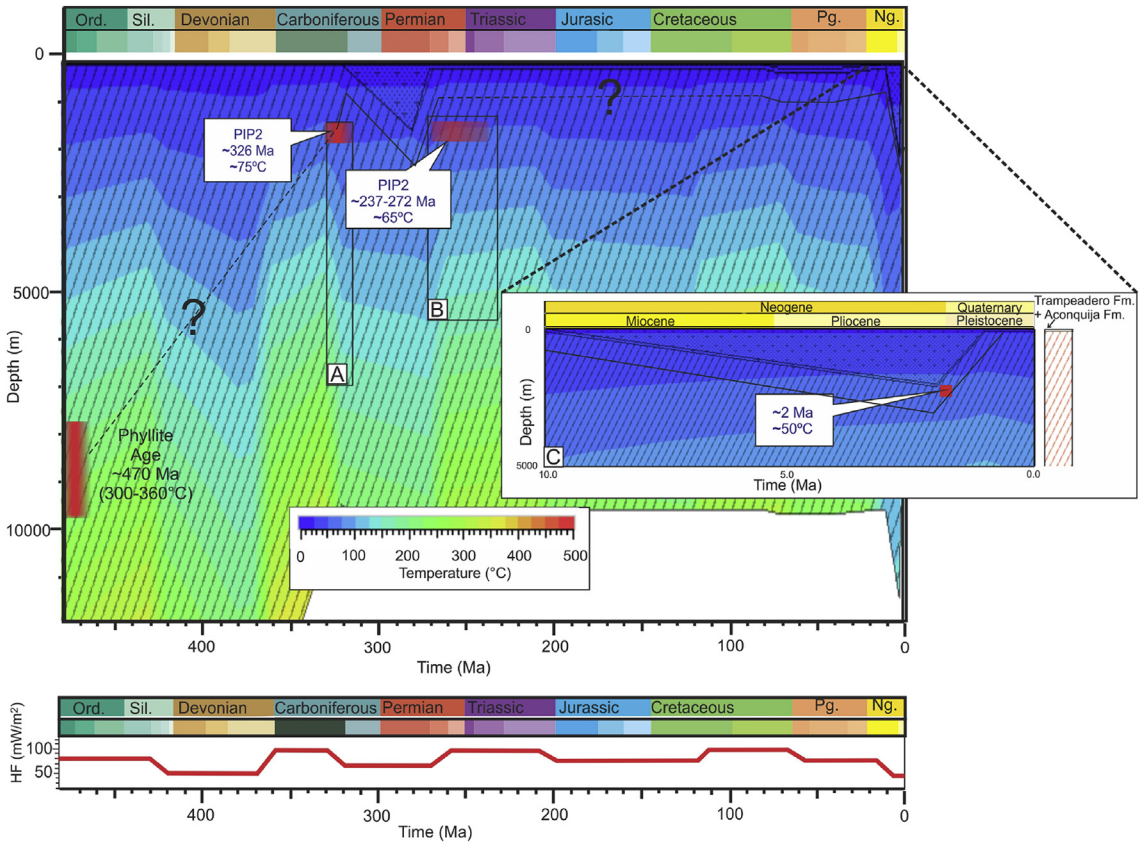

Fig. 11. Thermal modeling for Sierra de Ambato (sample PIP2) using PetroMod 1D Express software. For the different sedimentation episodes: continental with PWD zero and SWIT = ~22 °C. Heat flows estimated considering the different geotectonic context for the region from Paleozoic to present: normal subduction stage, 75 mW/m^2; flat subduction stage, 25 mW/m^2, transitional subduction stage, 65 mW/m^2; extensional regime 100 mW/m^2 [from Gutscher et al., 2000; Collo et al., 2011; Jaupart and Mareschal, 2007, Furlong and Chapman, 2013]. Thermal conductivity used to transform thermal gradients in heat flow values: 2.59 (W/mK) (from the software). Black boxes represent time-temperature constraint according to extrapolated K–Ar ages and clay mineral phases identified through XRD: A) illite temperature range between 100 and 300 °C (Merriman and Peacor, 1999; Vrolijk and van der Pluijm, 1999) at ~326 Ma; B) mixed-layer illite/smectite phases (R0-, R1-and R3-ordered) corresponds to temperatures 65–220 °C (Velde et al., 1986; Środoń, 2007) at ~ 237–272 Ma. Stratigraphically constrained sedimentation stages for the northern broken foreland are: 320–280 myr, 1200 m (Trampeadero Fm. and Permian units, González Díaz, 1970; Gutierrez and Barreda, 2006); 80–70 myr, 100 m (Cretaceous units, Mamani et al., 2002); and 10–2 myr, 2000 m (Aconquija Fm.), 1–0 myr, 5 m (Quaternary, Fisher et al., 2002; Mamani et al., 2002; González Díaz, 1970; Sobel and Strecker, 2003; Dávila et al., 2012). Time intervals are normal subduction stages, 200–120 myr and 60–20 myr; flat subduction stage, 420–370 myr and 10–1 myr; transitional subduction stage, 320–270 myr; extensional regime, 360–330 myr, 260–210 myr and 115–70 myr.

that authigenic clays in gouges occurred prior to the Mesozoic. No Cenozoic ages were obtained. Given the Paleozoic K–Ar ages recorded in modern faults, we propose successive reactivations since then, likely reworking the same weakness zone. The oldest age for the central damage zone suggests a deepest exhumation or the basement block kept relatively shallow since its exhumation in the Middle Paleozoic. The western and eastern fault zones record a Carboniferous exhumation likely associated with the relief formation and mountain building associated with the Late Paleozoic alpine glaciation in west-central Argentina. During Cenozoic deformational event, even though there is clear evidence of brittle deformation and exhumation in the study region, there is a lack of K–Ar ages that we attribute to the prevailing thermal regime instead of a minor exhumation event during this period.

Acknowledgements

We thank Consejo Nacional de Investigaciones Científicas y Técnicas (CONICET), Secretaría de Ciencia y Tecnología de la Universidad Nacional de Córdoba (SECyT-UNC), the IIF Marie Curie 7th Program (ERC) to support of our Research Projects in Argentina. We acknowledge the help of Geologist Nicolás Stoessel for assistance in various field campaigns and Juan Pablo Muñoz for lab assistance.

References

Aceñolaza, F.G., Miller, H., Toselli, A.J., 1996. Geología del Sistema de Famatina. In: Aceñolaza, F.G., Miller, H., Toselli, A.J. (Eds.), Geología del Sistema de Famatina. Münchner Geologische Hefte, Reihe A, vol. 9 (6), p. 412.

Aceñolaza, F.G., Miller, H., Toselli, A.J., 2000. Geología de la Sierra de Velasco, provincia de La Rioja, Argentina (en cd-rom), en 17. In: Geowissenschaftliches Lateinamerika – Kolloquium, Stuttgart, extended Abtracts: Profil, vol. 18, p. 38.

Alasino, P.H., Dahlquist, J.A., Pankhurst, R.J., Galindo, C., Casquete, C., Rapela, C.W., Larrovere, M.A., Fanning, C.M., 2012. Early Carboniferous sub– to mid–alkaline magmatism in the Eastern Sierras Pampeanas, NW Argentina: a record of crustal growth by the incorporation of mantle–derived material in an extensional setting. Gondwana Res. 22 (3–4), 992–1008.

Alvarado, P., Ramos, V.A., 2011. Earthquake deformation in the northwestern Sierras Pampeanas of Argentina based on seismic waveform modeling. J. Geodyn. 51, 205–218. http://dx.doi.org/10.1016/j.jog.2010.08.002.

Astini, R.A., 2009. El marco tectónico de la glaciación carbonífera. In: 12º Congreso Geológico Chileno, Actas S10-003: 9–12, Santiago.

Astini, R.A., Dávila, F.M., 2004. Ordovician retroarc foreland and Ocloyic thrust belt development on the western Gondwana margin as a response to the Precordillera terrane accretion. Tectonics 23, TC4008. http://dx.doi.org/10.1029/2003TC001620.

Astini, R.A., Tauber, A.A., Marengo, H.G., Oviedo, N., del, V., Martino, R., Guereschi, A., 2014. Cubierta cenozoica (Paleógeno–Neógeno) Relatorio de la geología y recursos Naturales de la Provincia de Córdoba (Cordoba).

Bense, F.A., Löbens, S., Dunkl, I., Wemmer, K., Siegesmund, S., 12/2013. Is the exhumation of the Sierras Pampeanas only related to Neogene flat-slab subduction? Implications from a multi-thermochronological approach. J. South Am. Earth Sci. 48, 123–144. http://dx.doi.org/10.1016/j.jsames.2013.09.002.

Bense, F., Wemmer, K., Löben, S., Siegesmund, S., 2014. Fault gouge analyses: K/Ar

illite dating, clay mineralogy and tectonic significance – A case study from the Sierras Pampeanas, Argentina. Int. J. Earth Sci. 103, 189–218. http://dx.doi.org/10.1007/s00531–013–0956–7.
Bossi, G.E., Muruaga, C.M., 2009. Estratigrafía e inversión tectónica del "rift" neógeno en el Campo del Arenal, Catamarca, NO Argentina. Andean Geol. 36 (2), 311–341.
Büttner, S.H., Glodny, J., Lucassen, F., Wemmer, K., Erdmann, S., Handler, R., Franz, G., 2005. Ordovician metamorphism and plutonism in the Sierra de Quilmes metamorphic complex: implications for the tectonic setting of the northern Sierras Pampeanas (NW Argentina). Lithosphere 83, 143–181. http://dx.doi.org/10.1016/j.lithos.2005.01.006.
Caelles, J.C., Clark, A.H., Farrar, E., McBride, S.L., Quirt, S., 1971. Potassium–argon ages of porphyry copper deposits and associated rocks in the Farallón Negro–Capillitas District, Catamarca. Argent. Econ. Geol. 66, 961–964. http://dx.doi.org/10.2113/gsecongeo.66.6.961.
Caminos, R., 1979. Sierras Pampeanas Noroccidentales Salta, Tucumán, Catamarca, La Rioja y San Juan. In: Turner, J.C. (Ed.), Segundo simposio de Geología Regional Argentina 1. Academia nacional de ciencias, Córdoba, pp. 225–291.
Carignano, C., Cioccale, M., Rabassa, J., 1999. Landscape antiquity of the central–eastern Sierras Pampeanas (Argentina): geomorphological evolution since Gondwanic times. Z. Geomorphol. 118, 245–268.
Carrapa, B., Hauer, J., Schoenbohm, L., Strecker, M.R., Schmitt, A.K., Villanueva, A., Sosa Gomez, J., 2008. Dynamics of deformation and sedimentation in the northern Sierras Pampeanas: an integrated study of the Neogene Fiambalá basin, NW Argentina. Geol. Soc. Am. Bull. 120 (11/12), 1518–1543.
Collo, G., Astini, R.A., Cawood, P.A., Buchan, C., Pimentel, M., 2009. U–Pb detrital zircon ages and Sm–Nd isotopic features in low–grade metasedimentary rocks of the Famatinian belt: implications for late Neoproterozoic – early Paleozoic evolution of the proto–Andean margin of Gondwana. J. Geol. Soc. Lond. 166 (2), 303–319.
Collo, G., Dávila, F.M., Nóbile, J.C., Astini, R.A., Gehrels, G., 2011. Clay mineralogy and thermal history of the Neogene Vinchina Basin, central Andes of Argentina: analysis of factors controlling the heating conditions. Tectonics 30, TC4012. http://dx.doi.org/10.1029/2010TC002841.
Collo, G., Dávila, F.M., Teixeira, Nóbile, J.C., Sańt Anna, L., Carter, A., 2015. Isotopic and thermochronologic evidence of an extremely cold lithosphere associated with a slab flattening. Basin Res. (in press).
Coughlin, T.J., O'Sullivan, P.B., Kohn, B.P., Holcombe, R.J., 1998. Apatite fission–track termochronology of the Sierras Pampeanas, central western Argentina: implications for the mechamism of plateau uplift in the Andes. Geology 26, 999–1002. http://dx.doi.org/10.1130/0091-7613(1998)026<0999:AFTTOT>2.3.CO;2.
Cristallini, E.O., Cominguez, A.H., Ramos, V.A., Mercerat, E.D., 2004. Basement doublewedge thrusting in the northern Sierras Pampeanas of Argentina Constraints from deep seismic reflection. In: McClay, K.R. (Ed.), Thrust Tectonics and Hydrocarbon Systems, vol. 82. American Association of Petroleum Geologists Memoir, pp. 65–90.
Dahlquist, J., Pankhurst, R., Rapela, C., Casquet, C., Fanning, C., Alasino, P., Baez, M., 2006. The San Blas Pluton: an example of Carboniferous plutonism in the Sierras Pampeanas, Argentina. J. South Am. Earth Sci. 20, 341–350.
Dahlquist, J.A., Alasino, P.H., Eby, G.N., Galindo, C., Casquet, C., 2010. Fault controlled Carboniferous A–type magmatism in the proto–Andean foreland (Sierras Pampeanas, Argentina): geochemical constraints and petrogenesis. Lithosphere 115, 65–81.
Dávila, F.M., Carter, A., 2013. Exhumation history of the Andean broken foreland revisited. Geology 41 (4), 443–446. http://dx.doi.org/10.1130/G33960.1.
Dávila, F.M., Lithgow-Bertelloni, C., 2013. Dynamic topography in South America. J. South Am. Earth Sci. 43, 127e144. http://dx.doi.org/10.1016/.
Dávila, F.M., Gimenez, M., Nóbile, J.C., Martinez, P.M., 2012. The evolution of the highelevated depocenters of the northern Sierras Pampeanas (ca. 28° SL), Argentine broken foreland, South–Central Andes: the Pipanaco Basin. Basin Res. 24, 1–22. http://dx.doi.org/10.1111/j.1365–2117.2011.00539.
Duarte, R.G., 1997. Gliptodontes del pleistoceno tardío de Agua de las Palomas, Campo del Pucara, Catamarca, Argentina. Variaciones morfológicas del caparazón de Glyptodon reticulatus Owen, 1845. Ameghiniana 34, 345–355.
Fernández Seveso, F., Tankard, A.J., 1995. Tectonics and Stratigraphy of the Late Paleozoic Paganzo Basin of Western Argentina and its regional implications. In: Tankard, A.J., Suárez S, R., Welsink, J. (Eds.), Petroleum Basins of South America, American Association of Petroleum Geologists, Memoir, vol. 62, pp. 285–301. Tulsa.
Fisher, N.D., Jordan, T.E., Brown, L., 2002. The structural and stratigraphic evolution of the La Rioja basin, Argentina. J. South Am. Earth Sci. 15, 141–156.
Fuhrmann, U., Lippolt, H.J., Hess, J.C., 1987. Examination of some proposed K–Ar standards: 40Ar/39Ar analyses and conventional K–Ar data. Chem. Geol. 66, 41–51.
Furlong, K.P., Chapman, D.S., 2013. Heat flow, heat generation, and the Thermal State of the Lithosphere. Annu. Rev. Earth Planet. Sci. Lett. 41, 385–410.
González Bonorino, F., 1950. Geología y Petrografía de las Hojas 12d (Capillitas) y 13d (Andalgalá). Bol. Dirección General Ind. Minera 70, 1–100 (Buenos Aires).
González Bonorino, F., 1953. Los supuestos depósitos de caolín en la falda occidental del Cordón Ambato (Catamarca). Rev. Asoc. Geol. 7 (3), 157–189.
González Díaz, E.F., 1970. El Carbónico Superior alto (Westfaliano–Estefaniano) de la quebrada de La Cébila (NE de La Rioja). In: 4ª Jornadas Geológicas Argentinas, Proceedings, vol. 2, pp. 163–186 (Mendoza).
González, O.E., 2000. Hoja Geológica 2766–2 San Miguel de Tucumán. SEGEMAR, Buenos Aires, p. 124.
Grathoff, G., Moore, D., Hay, R., Wemmer, K., 2001. Origin of illite in the lower Paleozoic of the Illinois Basin: evidence for brine migration. Geol. Soc. Am. Bull. 11, 1092–1104.
Grier, M., Salfity, J., Allmendinger, R., 1991. Andean reactivation of the Cretaceous Salta rift, Northwestern Argentina. J. South Am. Earth Sci. 4 (4), 351–372.
Grosse, P., Söllner, F., Báez, M.A., Toselli, A.J., Rossi, J.N., de la Rosa, J.D., 2009. Lower Carboniferous post–orogenic granites in central–eastern Sierra de Velasco, Sierras Pampeanas, Argentina: U–Pb monazite geochronology, geochemistry and Sr–Nd isotopes. Int. J. Earth Sci. 98 (5), 1001–1025.
Gutierrez, P.R., Barreda, V.D., 2006. Palinología de la Formación El Trampeadero (Carbonífero Superior), La Rioja, Argentina: significado bioestratigráfico. Ameghiniana. ISSN: 1851-8044 43 (1), 71–84.
Gutscher, M.–A., Spakman, W., Bijwaard, H., Engdahl, E.R., 2000. Geodynamics of flat subduction: Seismicity and tomographic constraints from the Andean margin. Tectonics 19 (5), 814–833. http://dx.doi.org/10.1029/1999TC001152.
Haines, S.H., van der Pluijm, B.A., 2008. Clay quantification and Ar–Ar dating of synthetic and natural gouge – Application to the Miocene Sierra Mazatán detachment fault, Sonora, Mexico. J. Struct. Geol. 30, 525–538.
Haines, S.H., van der Pluijm, B.A., 2010. Dating the detachment fault system of the Ruby Mountains, Nevada: significance for the kinematics of low-angle normal faults. Tectonics 29. http://dx.doi.org/10.1029/2009TC002552.
Harrison, T.M., Celerier, J., Aikman, A.B., Hermann, J., Heizler, M.T., 2009. Diffusion of ^{40}Ar in muscovite. Geochim. Cosmochim. Acta 73, 1039–1051.
Hayman, N.W., 2006. Shallow crustal fault rocks from the Black Mountain detachments, Death Valley, CA. J. Struct. Geol. 28, 1767e1784.
Heinrichs, H., Herrmann, A.G., 1990. Praktikum der Analytischen Geochemie. Springer, Berlin.
Hockenreiner, M., Sollner, F., Millar, H., 2003. Dating the TIPA shear zone: an Early Devonian terrane boundary between the Famatinian and Pampean systems (NW Argentina). J. South Am. Earth Sci. 16, 45–66. http://dx.doi.org/10.1016/S0895-9811(03)00018-X.
Hunziker, J.C., Frey, M., Clauer, N., Dallmeyer, R.D., Friedrichsen, H., Flehmig, W., Hochstrasser, K., Roggwiler, P., Schwander, H., 1986. The evolution of illite to muscovite: mineralogical and isotopic data from the Glarus Alps, Switzerland. Contributions Mineral. Petrol. 92, 157–218.
Husson, L., Conrad, C.P., Faccenna, C., 2012. Plate motions, Andean orogeny, and volcanism above the South Atlantic convection cell. Earth Planet. Sci. Lett. 317, 126–135. http://dx.doi.org/10.1016/j.epsl.2011.11.040.
Indri, D.A., Barber, L.E., 1987. Características geológicas y químicas del granito San Ignacio- Los Pinos, Provincias de Tucumán y Catamarca, Argentina. In: en 10° Congreso Geológico Argentino, San Miguel de Tucumán, vol. IV, pp. 135–138.
Isacks, B., Jordan, T., Allmendinger, R., Ramos, V.A., 1982. La segmentación tectónica de los Andes Centrales y su relación con la placa de Nazca subductada. In: 5° Congreso Latinoamericano de Geología, Actas, vol. 3, pp. 587–606.
Isbell, J.L., Henry, L.C., Gulbranson, E.L., Limarino, C.O., Fraiser, M.L., Koch, Z.J., Ciccioli, P.L., Dineen, A.A., 2012. Glacial paradoxes during the late Paleozoic ice age: evaluating the equilibrium line altitude as a control on glaciation. Gondwana Res. 22, 1–19.
Jaupart, C., Mareschal, J.–C., 2007. Heat flow and thermal structure of the lithosphere. In: Schubert, G. (Ed.), Treatise on Geophysics, vol. 6. Elsevier Ltd, Oxford, pp. 217–252.
Jordan, T.E., Allmendinger, R.W., 1986. The Sierras Pampeanas of Argentina: a modern analogue of Rocky Mountain foreland deformation. Am. J. Sci. 286, 737–764.
Jordan, T.E., Isacks, B.L., Allmendmger, R.W., Brewer, J.A., Ramos, V.A., Ando, C.J., 1983. Andean tectonics related to geometry of subducted Nazca plate. Bull. Geol. Soc. Am. 94, 341–361.
Jordan, T.E., Zeitler, P., Ramos, V.A., Gleadow, A.J.W., 1989. Thermochronometric data on the development of the basement peneplain in the Sierras Pampeanas, Argentina. J. S. Am. Earth Sci. 2, 207–222.
Kay, S.M., Abbruzzi, J.M., 1996. Magmatic evidence for Neogene lithospheric evolution of the central Andean "flat slab" between 30° and 32°S. Tectonophysics 259, 15–28.
Kisch, H.J., 1991. Illite crystallinity: recommendations on sample preparation, X-ray diffraction settings, and interlaboratory samples. J. Metamorph. Geol. 9 (6), 665–670. http://dx.doi.org/10.1111/j.1525-1314.1991.tb00556.x.
Kleidert, K., Strecker, M., 2001. Climate change in response to orographic barrier uplift: Paleosol and stable isotope evidence from the late Neogene Santa María basin, northwestern Argentina. Geol. Soc. Am. Bull. 113 (6), 728–742. http://dx.doi.org/10.1130/0016-7606(2001)113<0728:CCIRTO>2.0.CO;2.
Knüver, M., 1983. Dataciones radiométricas de rocas plutónicas y metamórficas. In: Aceñolaza, F.G., Miller, H., Toselli, A.J. (Eds.), La Geología de la Sierra de Ancasti: Münster, Münstersche Forschungen zur Geologie und Paläontologie, vol. 59, pp. 201–218.
Kralik, M., Klima, K., Riedmtiller, G., 1987. Dating fault gouges. Nature 327, 315–317.
Kübler, B., 1968. Evaluation quantitative du métamorphisme par la cristallinité d l'illite. Bull. Cent. Rech. Pau S.N.P.A. 2, 385–397.
Lanson, B., 1997. Decomposition of experimental X-Ray diffraction patterns (Profile fitting) a convenient way to study clay minerals. Clays Clay Miner. 45 (2), 132–146.
Lanson, B., Velde, B., 1992. Decomposition of X-ray diffraction patterns: a convenient way to describe complex US diagenetic evolution. Clays Clay Miner. 40, 629–643.
Larrovere, M.A., Toselli, A.J., Rossi de Toselli, J.N., 2008. Petrología y estructura de la

Faja de Deformación La Chilca, Catamarca Revista de la Asociación Geológica Argentina. Lugar, Buenos Aires, pp. 254–263.
Larrovere, M.A., de los Hoyos, C.R., Toselli, A.J., Rossi, J.N., Basei, M.A.S., Belmar, M.E., 2011. High T/P evolution and metamorphic ages of the migmatitic basement of northern Sierras Pampeanas. In: Argentina: Characterization of a Mid-crustal Segment of the Famatinian Belt. Journal of South American Earth Sciences, 31 (2–3), pp. 279–297.
Llambías, E., Quenardelle, S., Montenegro, T., 2003. The Choiyoi group from central Argentina: a subalkaline transitional to alkaline association in the craton adjacent to the active margin of the Gondwana continent. J. South Am. Earth Sci. 18, 243–257. http://dx.doi.org/10.1016/S0895–9811(03)00070–1.
Löbens, S., Bense, F.A., Wemmer, K., Dunkl, I., Costa, C.H., Layer, P., Siegesmund, S., 2010. Exhumation and uplift of the Sierras Pampeanas: preliminary implications from K–Ar fault gouge dating and low–T thermochronology in the Sierra de Comechingones (Argentina). Int. J. Earth Sci. Geol. Rundsch. 100, 671–694. http://dx.doi.org/10.1007/s00531–010–0608–0.
Löbens, S., Bense, F.A., Dunkl, I., Wemmer, K., Kley, J., Siegesmund, S., 2013. Thermochronological constraints of the exhumation and uplift of the Sierra de Pie de Palo, NW Argentina. J. South Am. Earth Sci. 48, 209e219.
Löbens, S., Sobel, E.R., Bense, F.A., Wemmer, K., Dunkl, I., Siegesmund, S., 2013. Refined exhumation history of the northern Sierras Pampeanas, Argentina. Tectonics 32, 1–20. http://dx.doi.org/10.1002/tect.20038.
Lyons, J.B., Snellenburg, J., 1971. Dating faults. Geol. Soc. Am. Bull. 82, 1749–1752.
Mamani, M., Castiglione, B., Buk, E., Degiuseppe, O., 2002. Determinación del Espesor Sedimentario en la Cuenca al Este de la Ciudad de La Rioja. XXI Reunión Científica AAGG Rosario (Argentina), pp. 202–207.
Merriman, R.J., Peacor, D.R., 1999. Very low-grade metapelites: mineralogy, microfabrics and measuring reaction progress. In: Frey, M., Robinson, D. (Eds.), Low-grade Metamorphism. Blackwell Science, Oxford, pp. 12–87.
Meunier, A., Velde, B., 2004. Illite: Origins, Evolution and Metamorphism. Springer, Berlin, p. 286.
Moore, D.M., Reynolds, R.C., 1997. X–Ray Diffraction and the Identification and Analysis of Clay Minerals. Oxford University Press, p. 378.
Mortimer, E.L., Carrapa, B., Coutand, I., Schoenbohm, L., Sobel, E.R., GomeZ, J.S., Strecker, M.R., 2007. Fragmentation of a foreland basin in response to out–ofsequence basement uplifts and structural reactivation: El Cajón–Campo del Arenal basin, NW Argentina. Geol. Soc. Am. Bull. 119 (5/6), 637–653.
Mpodozis, C., Ramos, V.A., 1989. The Andes of Chile and Argentina. In: Ericksen, G.E., Cañas Pinochet, M.T., Reinemud, J.A. (Eds.), Geology of the Andes and its Relation to Hydrocarbon and Mineral Resources, Circumpacific Council for Energy and Mineral Resources, Earth Sciences Series, vol. 11, pp. 59–90.
Murra, J.A., Baldo, E.G., Galindo, C., Casquet, C., Pankhurst, R.J., Rapela, C.W., Dahlquist, J., 2011. Sr, C and O isotope composition of marbles from the Sierra de Ancasti, Eastern Sierras Pampeanas. Argentina age constraints Neoproterozoic-Lower Paleoz. Evol. Proto-Gondwana Margin Geol. Acta 9 (1), 79–92.
Nasif, N.L., Esteban, G., Georgieff, S.M., 2007. Nuevo registro de vertebrados para la Formación Aconquija, provincia de Catamarca, Noroeste de Argentina. Implicancias cronoestratigráficas y consideraciones paleoambientales. Acta Geol. Llilloana 20 (1), 99–112.
Nóbile, J.C., Dávila, F.M. Quantifying uplift in the northern argentine broken foreland using longitudinal river profiles.in prep.
Pankhurst, R.J., Rapela, C.W., 1998. The Proto- Andean margin of Gondwana: an introduction. In: Pankhurst, R.J., Rapela, C.W. (Eds.), The Proto- Andean Margin of Gondwana, Geological Society of London, pp. 1–9. Special Publications 142.
Pankhurst, R.J., Rapela, C.W., Fanning, C.M., 2000. Age and origin of coeval TTG, I- and S-type granites in the Famatian belt of NW Argentina. Trans. R. Soc. Edinb. Earth Sci. 91, 151–168.
Passchier, C.W., Trouw, R.A., 2005. Microtectonics, second ed. Springer-Verlag Berlin, Heidelberg, p. 366.
Pevear, D.R., 1992. Illite age analysis, a new tool for basin thermal history analysis. In: Maest, A.S., Kharaka, Y.K. (Eds.), Water-rock Interaction. AA Balkema, Rotterdam, pp. 1251–1254.
Purdy, J.W., Jager, E., 1976. K-Ar Ages of Rock Forming Minerals from the Central Alps. Inst. Geol. Min. Univ. Padeava, Mere, p. 30.
Ramos, V.A., Kay, S.M., 1991. Triassic rifting and associated basalts in the Cuyo basin, central Argentina. In: Harmon, R.S., Rapela, C.W. (Eds.), Andean Magmatism and its Tectonic Setting. Geological Society of America, Boulder, pp. 79–91. Special Paper 265.
Ramos, V., Cristallini, E.O., Pérez, D.J., 2002. The Pampean flat-slab of the Central Andes. J. S. Am. Earth Sci. 15, 59–78.
Rapela, C.W., Pankhurst, R.J., Casquet, C., Baldo, E., Saavedra, J., Galindo, C., Fanning, C.M., 1998. The Pampean Orogeny of the southern proto-Andes: Cambrian continental collision in the Sierras de Córdoba. In: Pankhurst, R.J., Rapela, C.W. (Eds.), The Proto-Andean Margin of Gondwana, pp. 179–217. Geological Society Special Publication, 142.
Rapela, C.W., Fanning, C.M., Baldo, E.G., Dahlquist, J.A., Pankhurst, R.J., Murra, J.A., 2005. Coeval S- and I- type granites in the Sierra de Ancasti, Eastern Sierras Pampeanas, Argentina. Gondwana. In: Pankhurst, R., Veiga, G. (Eds.), Gondwana 12, Geological and Biological Heritage of Gondwana, Academia Nacional de Ciencias, Abstracts: 307, Córdoba.
Rapela, C.W., Pankhurst, R.J., Casquet, C., Fanning, C.M., Baldo, E.G., González-Casado, J.M., Galindo, C., Dahlquist, J., 2007. The Río de la Plata craton and the assembly of SW Gondwana. Earth Sci. Rev. 83, 49–82.
Reiners, P.W., Ehlers, T.A., Zeitler, P.K., 2005. Past, present and future of thermochronology. Rev. Mineral. Geochem. 58, 118.
Rossello, E.A., Mozetic, M.E., 1999. Caracterización estructural y significado geotectónico de depocentros cretácicos continentales del centro-oeste argentino, en Boletim do 5° Simpósio o Cretáceo do Brasil: 107–113. UNESP, Campus de Rio Claro/São Paulo.
Rossi, J.N., Toselli, A.J., Saavedra, J., Sial, A.N., Pellitero, E., Ferreira, V.P., 2002. Common crustal source for contrasting peraluminous facies in the early Paleozoic Capillitas Batholith. NW Argentina Gondwana Res. 5 (2), 325–337.
Schumacher, E., 1975. Herstellung von 99, 9997% 38Ar für die 40K/40Ar Geochronologie. Geochronol. Chim. 24, 441–442.
Sibson, R.H., 1977. Fault rocks and fault mechanisms. J. Geol. Soc. I33, 191–213.
Sims, J.P., Ireland, T.R., Camacho, A., Lyons, E., Pieters, P.E., Skirrow, R.G., Stuart-Smith, P.G., Miró, R., 1998. U-Pb, Th-Pb and Ar-Ar geochronology from the southern Sierras Pampeanas, Argentina: implications for the Palaeozoic tectonic evolution of the western Gondwana margin. In: Pankhurst, R.J., Rapela, C.W. (Eds.), The Proto-Andean Margin of Gondwana, pp. 259–281.
Sobel, E.R., Strecker, M.R., 2003. Uplift, exhumation and precipitation: tectonic and climatic control of Late Cenozoic landscape evolution in the northern Sierras Pampeanas, Argentina. Basin Res. 15, 431–451.
Solum, J.G., van der Pluijm, B.A., Peacor, D.R., 2005. Neocrystallization, fabrics and age of clay minerals from an exposure of the Moab fault. Utah J. Struct. Geol. 27, 1563–1576. http://dx.doi.org/10.1016/j.jsg.2005.05.002.
Środoń, J., 2007. Illitization os smectite and history of sedimentary basins. In: EUROCLAY Conference, Aveiro, Portugal, pp. 74–82.
Steenken, A., Wemmer, K., López de Luchi, M.G., Siegesmund, S., Pawlig, S., 2004. Crustal Provenance and cooling of the basement complexes of the Sierra de San Luis: an insight into the tectonic history of the Pro to–Andean margin of Gondwana. Gondwana Res. 7 (4), 1171–1195. http://dx.doi.org/10.1016/S1342–937X(05)71092–3.
Steenken, A., Siegesmund, S., Wemmer, K., López de Luchi, M.G., 2008. Time constraints on the Famatinian and Achalian structural evolution of the basement of the Sierra de San Luis (Eastern Sierras Pampeanas, Argentina). J. South Am. Earth Sci. 25 (3), 336–358. http://dx.doi.org/10.1016/j.jsames.2007.05.002.
Steenken, A., Wemmer, K., Martino, R.D., López de Luchi, M.G., Guereschi, A., Siegesmund, S., 2010. Post–Pampean cooling and the uplift of the Sierras Pampeanas in the west of Córdoba (Central Argentina). N. Jb Geol. Pal A 256 (2), 235–255. http://dx.doi.org/10.1127/0077–7749/2010/0094.
Steiger, R.H., Jaeger, E., 1977. Subcommission on geochronology; convention on the use of decay constants in geo- and cosmochronology. Earth Planet. Sci. Lett. 36 (3), 359–362.
Strecker, M.R., Cerveny, P., Bloom, A.L., Malizia, D., 1989. Late Cenozoic tectonism and landscape development in the foreland of the Andes: Northern Sierras Pampeanas. Argent. Tect. 8, 517–534. http://dx.doi.org/10.1029/TC008i003p00517.
Szczerba, M., Środoń, J., 01/2009. Extraction of diagenetic and detrital ages and of the ^{40}K Detrital/^{40}K diagenetic ratio from KAr dates of Clay fractions. Clays Clay Miner. 57 (1), 93–103.
Tauber, A.A., 2002. Parque Geológico Sanagasta, una nueva área protegida de la provincia de La Rioja, Argentina. 1° Congreso Internacional: Patrimonio Cultural (Córdoba), pp. 471–483. Actas en CD–R.
Toselli, A.J., 1992. El magmatismo del noroeste argentino. Reseña sistemática e interpretación: San Miguel de Tucumán, Universidad Nacional de Tucumán. Ser. Correlación Geol. 8, 243.
Toselli, G.A., 1983. Petrografía del stock granitoide de Las Juntas y metamorfitas encajantes, Sierra de Ambato, provincia de Catamarca: Revista de la Asociación Argentina de Mineralogía. Petrol. Sedimentol. 14 (1–2), 15–24.
Toselli, A.J., Aceñolaza, F.G., Rossi de Toselli, J.N., 1986. A proposal for the systematization of the Upper Precambrian – Lower Palaezoic Basament in the Sierras Pampeanas, Argentina. Z. Geol. Paläontol. Teil I, 9(10), 1227–1233.
Toselli, A.J., Sial, A.N., Saavedra, J., Rossi de Toselli, J.N., Pinto Ferreira, V., 1996. Geochemistry and genesis of the S type, cordierite-andalusite-bearing Capillitas Batholith. Argent. Int. Geol. Rev. 38 (11), 1040–1053.
Uliana, M.A., Biddle, K.T., Cerdán, J., 1989. Mesozoic extension and the formation of Argentine sedimentary basins. In: Tankard, A.J., Balkwill, H.R. (Eds.), Extensional Tectonics and Stratigraphy of the North Atlantic Margins, vol. 46. American Association of Petroleum Geologist, Memoir, pp. 599–614.
van der Pluijm, B.A., Hall, C.M., Vrolijk, P.J., Pevear, D.R., Covey, M.C., 2001. The dating of shallow faults in the Earth's crust. Nature 412, 172–175.
van der Pluijm, B.A., Vrolijk, P.J., Pevear, D.R., Hall, C.M., Solum, J., 2006. Fault dating in the Canadian Rocky Mountains: evidence for late Cretaceous and early Eocene orogenic pulses. Geology 34, 837–840. http://dx.doi.org/10.1130/G22610.1.
Vázquez, F., 2010. Geología y estratigrafía neógena en la Quebrada del río Las Lajas Bolsón de Zapata), Catamarca: Suimportancia para entender la evolución tectonoestratigráfica en el antepaís fragmentado. Universidad Nacional de Córdoba, Argentina. Tesis de grado (inédita).
Velde, B., Suzuki, T., Nicot, E., 1986. Pressure-temperature-composition of illite/smectite mixed-layer minerals: Niger delta mudstones and other examples. Clays Clay Miner. 34 (4), 435–441.
Verdecchia, S.O., Baldo, E.G., 2010. Geoquímica y procedencia de los metasedimentos ordovícicos del complejo metamórfico La Cébila, provincia de La Rioja, Argentina. Rev. Mex. Ciencias Geol. 27 (1), 97–111.
Verdecchia, S.O., Collo, G., Baldo, E.G., 2011. Polyphase white mica growth in low-grade metapelites from La Cébila Metamorphic Complex (Famatinian Belt, Argentina): evidence from microstructural and XRD investigations. Andean Geol. 38 (2), 268–283.

Vrolijk, P., van der Pluijm, B.A., 1999. Clay Gouge J. Struct. Geol. 21, 039–1048. http://dx.doi.org/10.1016/S0191–8141(99)00103–0.
Wart, L.N., Rice, A.H.N., 1994. Interlaboratory standardization and calibration of clay mineral crystallinity and crystallite size data. J. Metamorph. Geol. 12, 141–152.
Wemmer, K., Ahrendt, H., 1997. Comparative K/Ar and Rb/Sr age determination of retrograde processes on rocks from the KTB deep drilling project. Geol. Rundsch 86 (Suppl. l), S272–S285.
Ylagan, R., Kim, C., Pevear, D., Vrolijk, P., 2002. Illite polytype quantification for accurate K–Ar determination. Am. Mineral. 87, 1536–1545.
Zwingmann, H., Mancktelow, N.S., 2004. Timing Alp. Fault Gouges Earth Planet. Sci. Lett. 223, 415–425. http://dx.doi.org/10.1016/j.epsl.2004.04.041.